Contents lists available at *Dergipark*

International Journal of Boron Science and Nanotechnology

journal homepage :https://dergipark.org.tr/en/pub/ijbsn

Number 1, December 2024

RESEARCH ARTICLE

Received Date: 23.12.2024 *Accepted Date: 30.12.2024*

Determination of the solid solubility limit of iron atom from different sources, in the mullite crystals, obtained from illitic/kaolinitic clays

Zeynep Gizem Saritas[a,c], Rasim Ceylantekin[a*], Merve Akin[a,b], Güray Kaya[a], Fatih Sen[b]

[a] *Department of Material Science and Engineering, Dumlupınar University, 43100, Kutahya, Türkiye*
[b]*Sen Research Group, Department of Biochemistry, Dumlupinar University,43100, Kutahya, Türkiye*
[c]*Keramika Research Group, Keramika Ceramics, Ünsa Mining, Tourism, Energy, Ceramics, Forest Products, Electricity Production Industry, 43100, Kutahya, Türkiye*

Abstract

This study: aims to bring clay, which is one of the important raw materials of the ceramic and porcelain sectors, to the production of soft porcelain in a cleaner and higher quality way. In addition, this study aims to prevent the discoloration of iron, which is present in high ratios in clays used in the traditional ceramic industry. In the study, two types of iron were added to CC-31 clay; Fe_2O_3 at 0 %, 2 %, 4 %, 6 %, 8 %, 10 % by weight and $FeCl_3$ at 0 %, 4.05 %, 8.1 %, 12.16 %, 16.21 %, 20.26 % by weight. At this point, FeO will be broken down as Fe enters the crystal structure and the coloring effect will be prevented. XRF (X-ray Fluorescence), XRD (X-ray Diffraction), and TG/DTA (Thermal Gravimetry/Differential Thermal Analysis) analyses were performed to determine the chemical properties and thermal properties of CC-31 clay used in the study. Density, water absorption, and porosity tests were performed. L*a*b* (3D color coordinates) values were measured for the samples prepared and sintered with CC-31 clay. In addition, the effect of iron addition to CC-31 clay was investigated on the sintered samples by XRD analysis, the surface images, and the growth of mullite crystals by SEM (Scanning Electron Microscopy) analysis. In addition, the crystal parameters of mullite were calculated and the iron solubility limit in mullite was determined. The results showed that the hematite phase started to appear with the addition of 6% of both iron sources, and the mullite phase formed after sintering at 1200 ºC could dissolve iron up to 4-5% addition. Within the scope of the study, it has been shown that CC-31 clay can be used in the porcelain / ceramic industry and that it provides a high advantage with its high mullitization rate and will host a high mullitization rate.

* Corresponding author.
E-mail address: rasim.ceylantekin@dpu.edu.tr

Keywords: Clay; Iron; Mullite; Solubility of Iron.

1. Introduction

The rapid growth in the ceramic and porcelain sector in the world increases the consumption of raw materials used in the production of these materials [1], [2]. One of the most important raw materials used in this sector is clay. Clays are naturally white, gray, brown, yellow, red, and black; however, these colors change during firing [3]. A clay that is red, black, or brown in its natural state can turn white after sintering [4]. The substances that affect the firing color the most are the compounds containing Fe (iron), Mg (manganese), and TiO_2 (titanium oxides) ink the clays. Furthermore, as the sintering temperature increases during firing, the color composition may also increase. These color changes are important parameters for the ceramic and porcelain sectors. It is very important to provide a clean, and white production for these sectors [5]. In this context, there are impurities in the clays used in ceramics and porcelains where a white, and clean production is desired. The main impurities are elements such as Aluminum (Al), Silicon (Si), Fe, Calcium (Ca), Sodium (Na), Magnesium (Mg), and Potassium (K). These elements can enter the structure of clays and cause undesirable effects in production. Especially impurities such as Iron Oxide (Fe_2O_3) can have significant side effects such as physical, chemical, and aesthetic appearance. To reduce side effects such as coloring in ceramics, and porcelains, mullite crystals can be formed in the structure and Fe can be trapped in mullite crystals [6], [7], [8], [9], [10]. Mullite's properties such as resistance to high temperatures and high corrosion resistance have increased its use in the ceramic industry. Natural mullite contains Fe and sometimes chromium as foreign components [11], [12], [13]. This foreign cation content is generally known to be low, and the presence of mullite rich in Fe_2O_3 and TiO_2 has also been described. Literature studies in this context have shown that mullite contains up to about 12% Fe_2O_3 [14], [15]. Incorporation of iron into mullite results in relatively low lattice, but stronger b lattice and c lattice constant expansions [16],[17]. In addition, microscope analysis shows that iron is enriched at the outer edges of the mullite, while the areas of the inner crystals contain less Fe [17], [18], [19].

Within the scope of this study, studies were carried out to prevent the coloration of Fe, which is encountered at high rates in clays frequently used in the ceramic and porcelain sectors. It has been observed that physical/chemical instability and color changes can be prevented with the mullite crystals formed.

2. Materials and methods

CC-31 clay was used as the raw material. In addition, Iron (III) Oxide (Fe_2O_3) and Iron (III) Chloride ($FeCl_3$) were used as iron sources. The samples were pressed into a 40 Ømm dye with 3N after moistening with 5 wt % of water. The pressed samples were dried at 80 ºC in a NAVY –FN-500 drier and then sintered in MSE _M1300 furnace at 1200 ºC for 3 hours. Heating and cooling rates were 5 ºC/min.

2.1. Materials characterization

To determine the chemical properties of CC-31 clay, XRF (X-ray Fluorescence) analyses were performed with a Panalytical/Axios MAX spectrometry, and TG/DTA (Thermal Gravimetry/ Differential Thermal Analysis) analyses were performed with SETARAM/labSys evo brand device to determine its thermal properties. XRD (X-ray Diffraction) analysis was performed for raw clay and fired samples with a Panalytical Epmyrean brand device. For the XRD data collection, the samples were scanned between 10º-70º (2θ) with 0.02 step size and 0.04 radian Soller slits and ½" and ¼ "anti-scatter slits. The International Crystal Structure Database (ICSD) was used for the phase identification. Quantitative phase analysis of the samples was calculated with the Rietveld method using HighScore plus software (Panalytical, License Number:100 4501). The refined pattern of the sample with 2% wt of Fe_2O_3 was given in Fig.1. Then, density, water absorption, and porosity tests of the fired samples were carried out with standard Archimedes and water absorption methods. L*a*b* values were measured with an X-Rite spectrophotometer. The microstructure of the fractured surfaces was analyzed with FEI Nova Nano SEM 650 after etching with %10 HCl. With this analysis, crystallographic and morphological examinations of the samples, as well as elemental examinations were made. The raw materials used are given in Fig. 2 and the formulations are given in Table 1. The pictures of the raw materials used are given in Fig. 2 and the formulations are given in Table 1.

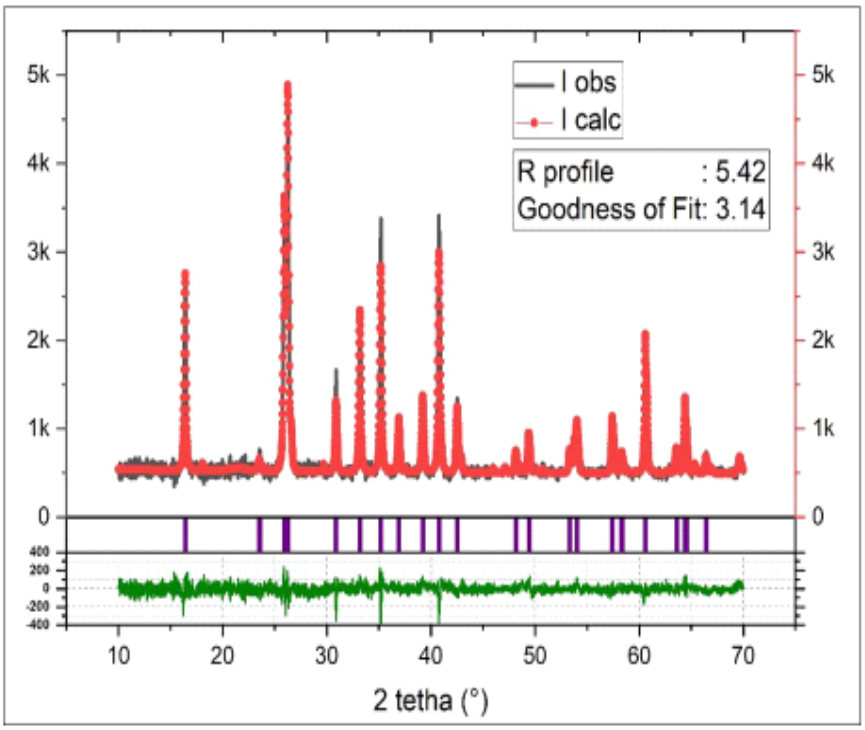

Fig 1. Rietveld plot of samples.

Fig 2. Raw materials used; (a) CC-31 clay; (b) Fe_2O_3; (c) $FeCl_3$.

Table 1. Prepared formulations (% by weight).

Materials	1	2	3	4	5	6	7	8	9	10	11	12
CC-31 Clay	100	100	100	100	100	100	100	100	100	100	100	100
Fe_2O_3	0	2	4	6	8	10						
$FeCl_3$							0	4.05	8.1	12.16	16.21	20.26

3. Results and discussion

Elemental analysis was first performed for the CC-31 clay used in this study and is given in Table 2. 47.23% SiO_2, and 36.61% Al_2O_3 were in the detected clay and the amount of iron was quite low. The high amount of Al_2O_3 and low Fe_2O_3 and TiO_2 ratios provide advantages in terms of usability in the porcelain applications.

Table 2. Elemental analysis results of CC-31 clay.

Components	SiO_2	Al_2O_3	K_2O	Fe_2O_3	MgO	BaO	P_2O_5	TiO_2	Na_2O	CaO	Less on ignition (%)
(%)	47.23	36.61	2.46	0.92	0.38	0.14	0.09	0.07	0.06	0.06	11.8
Components	Cl	Kb_2O	SO_3	CuO	PbO	ZrO_2	ZnO	NiO	CrO_3		Total (%)
(%)	0.05	0.04	0.03	0.02	0.02	0.02	0.01	0.03	0.02		100.01

The result of the XRD analysis of CC-31 clay is shown in Fig. 3 and the results of quantitative analysis are shown in Table 3. According to the XRD results obtained, mineral analysis of raw CC-31 clay showed that kaolinite (ICSD # 98-006-8698), muscovite (ICSD # 98-007-7497), and quartz (ICSD # 98-007-0007) were present in the raw material. The results showed that kaolinite was the main phase with 74.5%.

Table 3. Quantitative analysis data of CC-31 clay.

Phases	% by weight
Quartz	5.6
Kaolinite	74.5
Muscovite	19.9
Total	100

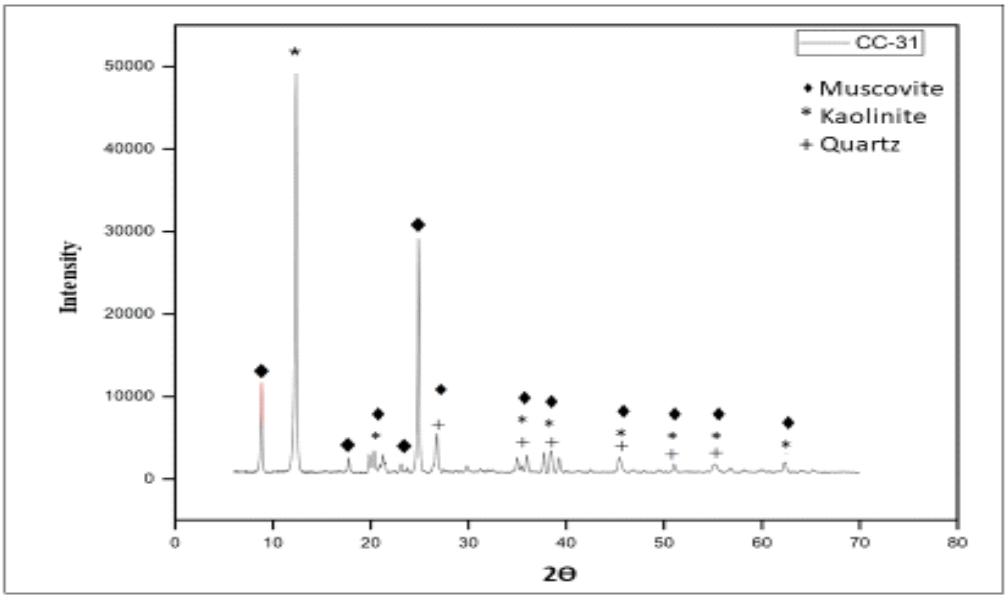

Fig 3. XRD patterns of CC-31 clay.

Fig. 4 shows the TG/DTA graph of CC-31 clay. When the DTA curve was examined, physical water was removed at 100 ºC and organic materials began to burn out at approximately 250 ºC. An endothermic peak occurred at 537 ºC and indicated the removal of $[OH]^-$ group molecules from the body. The exothermic peak at 987 ºC is due to the formation of new minerals, particularly primary mullite. In the TG curve, it is seen that there is no weight loss up to 350 ºC and it starts to decompose after this temperature. A rapid weight loss occurred in the temperature range of 350-850 ºC. The weight remains constantly above 850 ºC.

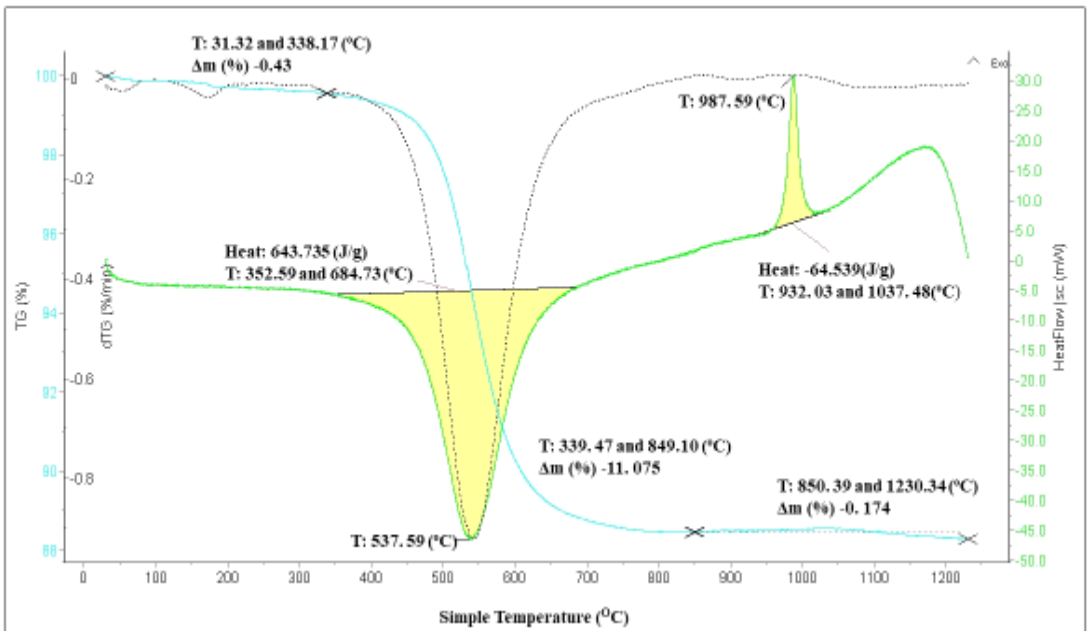

Fig 4. TG/ DTA graphic of CC-31 clay.

The density, water absorption, and porosity values of samples sintered at 1200 ºC are given in Table 4. It was observed that the water absorption and porosity values decreased with the addition of Fe_2O_3 and $FeCl_3$ compared to CC-31 clay without additives. The reason for this; is because, with increasing iron content, iron begins to act as a flux at higher temperatures. It was observed that the density values did not change much according to the added iron sources and their ratios.

Table 4. Density, water absorption, and porosity values of samples.

Prescription No	%Water Absorption	% Porosity	Intensity	Prescription No	% Water Absorption	% Porosity	Intensity
1	2.35	5.69	2.42	7	2.35	5.69	2.42
2	0.22	0.56	2.56	8	0.67	1.69	2.75
3	0.21	0.57	2.65	9	0.48	1.23	2.6
4	0.31	0.82	2.68	10	0.33	0.88	2.65
5	0.21	0.56	2.72	11	0.36	0.95	2.67
6	0.11	0.29	2.72	12	0.75	2.01	2.67

L*a*b* results of samples with different formulations sintered at 1200 ºC are given in Table 5. It is seen that the L* value of CC-31 clay is quite high (sample#1). The whiteness decreased proportionally with the added iron ratios. In addition to these, the greenness increased (a* value) as iron was added. At higher iron contents, free iron enters the glassy phase and causes the color to turn green.

Table 5. L*a*b* values of the formulations.

Formulations Number	L*	a*	b*	Formulations Number	L*	a*	b*
1	91.36	0.3	9.22	7	91.36	0.3	9.22
2	68.86	2.17	11.38	8	76.03	1.78	13.8

3	50.07	6.59	6.88	9	38.59	27.68	23.49
4	41.61	14.51	7.96	10	40.02	26.17	21.66
5	40.22	18.42	11.92	11	39.23	23.88	18.23
6	37	22.42	15.57	12	38.75	20.84	14.72

The quantitative analysis of the formulations is given in Table 6. Considering the data of CC-31 clay, it is seen that the mullite ratio was high. At the same time, the amount of cristobalite was quite low. Considering these features, its use in the ceramic/ porcelain sector is very advantageous. It was observed that the amount of quartz decreased and the amount of cristobalite increased as the amount of mullite decreased with the gradual addition of iron. This situation: showed that iron not only entered the mullite structure, but also entered the quartz structure, and enabled the conversion of quartz to cristobalite. It is thought that the low cristobalite ratio for this clay type will not constitute a disadvantage. At the same time, it was seen that the hematite ratio did not change until the addition of 6% in both iron source additions and started to increase after 6% wt. At the same time, for both iron sources, hematite was not significant up to 6% of iron addition and started to increase thereafter.

In Fig. 5 XRD patterns of the samples with sequentially added % Fe_2O_3 and % $FeCl_3$ into CC-31 clay were given. It was observed that the mullite peaks shifted to lower angles with the addition of both iron sources up to 6%. This was supported by lattice parameters, expansion rate, and crystal growth (Fig. 7-8-12). The Hematite peak did not appear until 6% of iron addition for both iron sources (Upper right side of Fig. 5). Therefore, it could be said that the iron atom could incorporate in the mullite crystal structure up to 4% and begin to form hematite as an individual phase. This was also supported by the quantitative analysis data in Table 6.

Table 6. Quantitative analysis data of CC-31 clay.

Formulation Number	Mullite	Quartz	Total Cristobalite	Magnetite	Hematite	Total
1	94.10	5.07	0.83	0.00	0.00	100.00
2	94.78	4.43	0.18	0.59	0.01	99.99
3	93.85	4.63	0.26	0.92	0.34	100.00
4	92.73	4.25	0.18	0.97	1.87	100.00
5	90.17	3.98	0.17	1.09	4.60	100.01
6	88.50	1.79	0.90	1.26	7.55	100.00
7	94.10	5.07	0.83	0.00	0.00	100.00
8	93.67	5.63	0.41	0.29	0.00	100.00
9	93.56	4.72	1.08	0.07	0.57	100.00
10	92.63	3.67	0.59	0.99	2.12	100.00
11	88.84	4.97	0.61	0.97	4.61	100.00
12	83.13	3.89	1.05	1.19	10.74	100.00

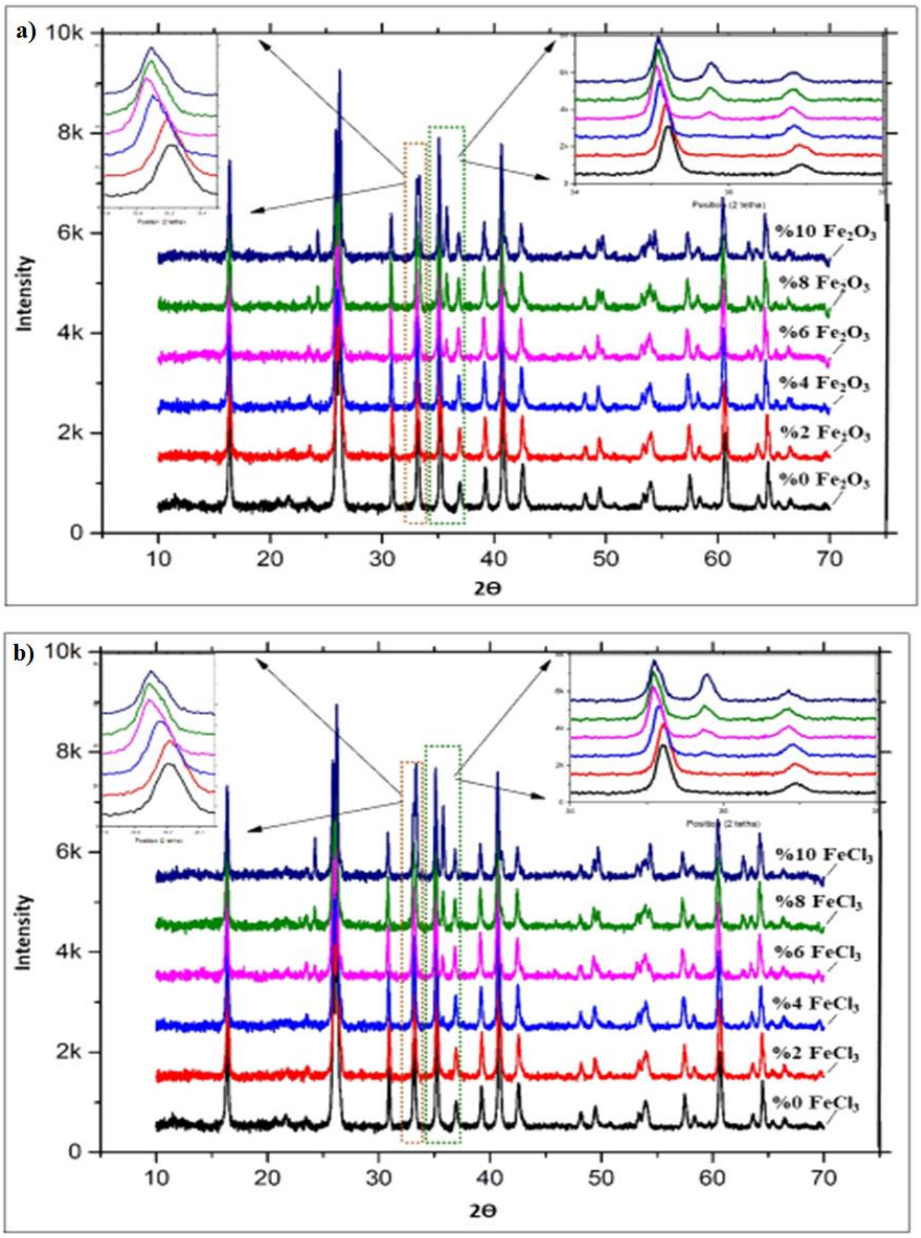

Fig 5. XRD patterns of CC-31 clay after sintering 1200 ºC with the addition of (a) Fe_2O_3; (b) $FeCl_3$.

In Fig. 6 the development of the hematite phase depending on the amount of Fe_2O_3 and $FeCl_3$ addition to the clay by weight percent were given. For Fe_2O_3 addition (Fig.6a), hematite began to be seen in the structure with the addition of 6% Fe_2O_3 and this ratio was 1.87 (Table 6). With the addition of 8% and 10% Fe_2O_3, the hematite ratio increased to 4.6 and 7.55, respectively. In the case of $FeCl_3$ (Fig.6b), a small amount of hematite began to be seen after 4% addition. With the addition of 6%, 8%, and 10% $FeCl_3$, the hematite ratio was determined as 2.16%- 4.61% and 10.74%, respectively. According to these results, $FeCl_3$ addition causes higher hematite formation than Fe_2O_3.

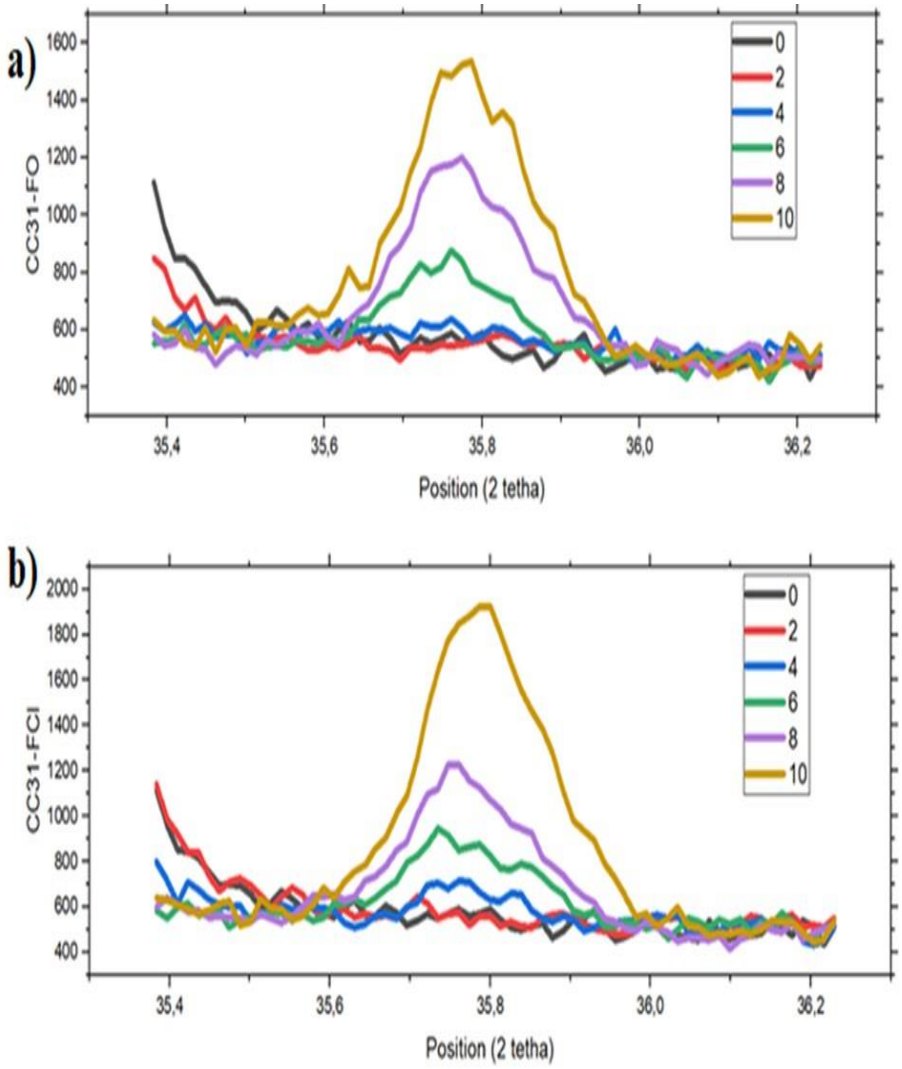

Fig 6. The development of hematite depends on the amount of (a) Fe_2O_3; (b) $FeCl_3$.

In Fig. 7 the lattice parameters of the mullite were given as Fe_2O_3 and $FeCl_3$ were added gradually into the CC-31 clay. It was observed that all of the mullite lattice parameters increased up to 8% of iron addition and remained constant thereafter.

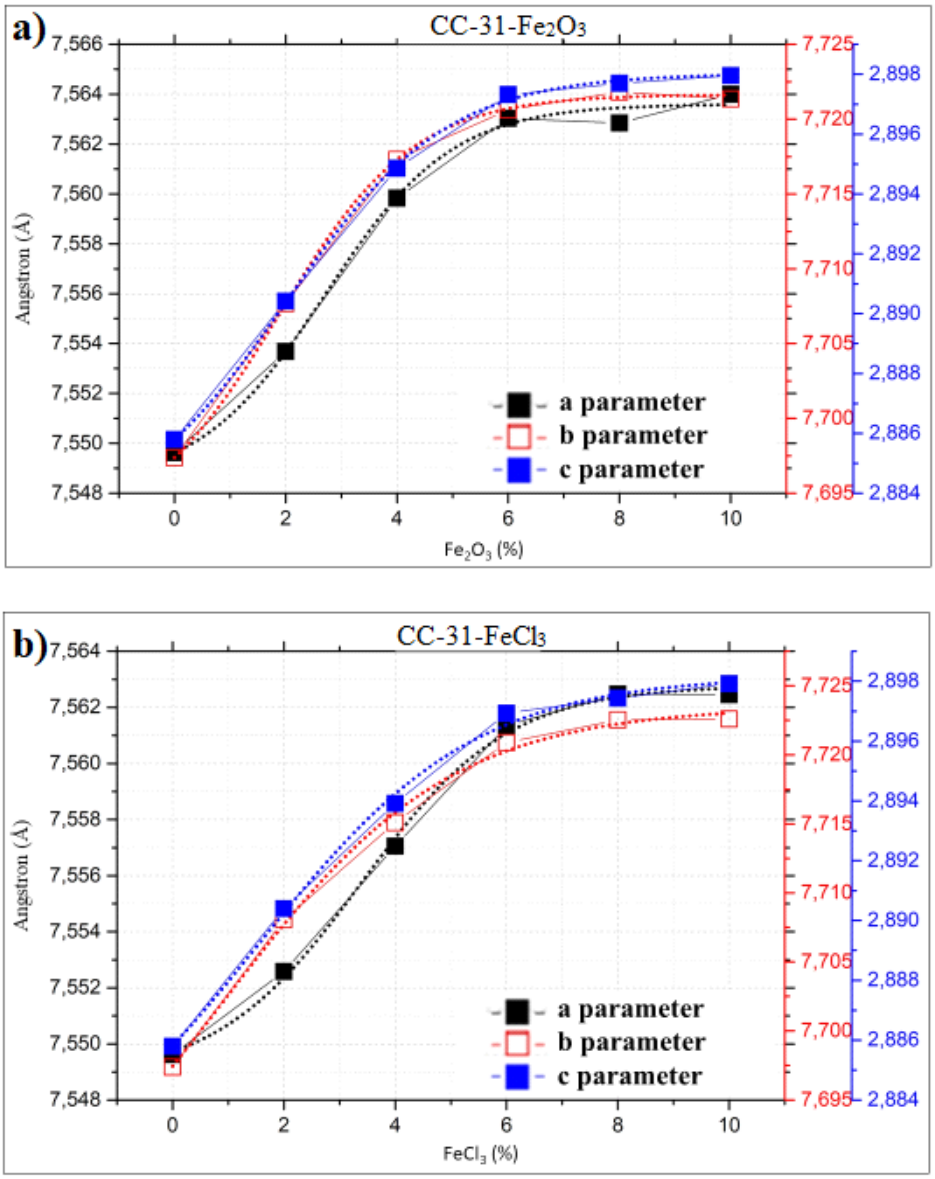

Fig 7. Lattice parameters of mullit phase after adding (a) Fe_2O_3; (b) $FeCl_3$.

In Fig. 8 the expansion rates of the lattice parameters of the mullite were given by gradually adding wt% Fe_2O_3 / $FeCl_3$ into the CC-31 clay. It was seen that there is a rapid expansion up to 6% with the addition of Fe_2O_3 and $FeCl_3$, and the expansion rate remains almost constant with the addition of more iron. The expansion rate of the c parameter was higher than the expansion rates of the a and b parameters in both iron source additions, which indicated that the iron atom incorporated into the mullite lattice in the c-direction.

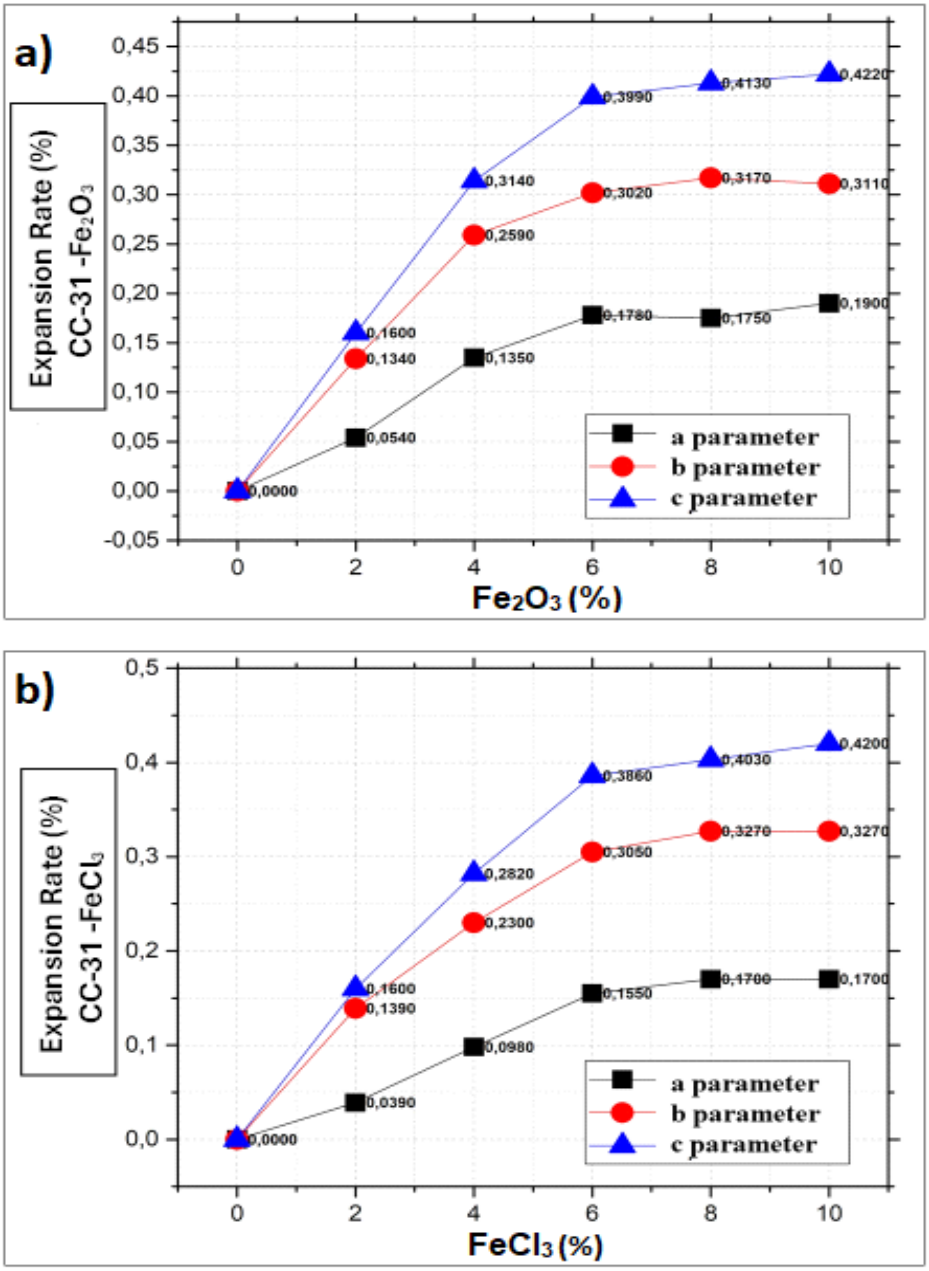

Fig 8. Expansion rate of lattice parameters of mullite in (a) Fe_2O_3; (b) $FeCl_3$ added CC-31 clay.

A wide variety of transition metal cations can replace the Al^{3+} ion in tetrahedral or octahedral regions in the mullite lattice forming solid solutions (Fig.9) [7]. In this context, the solubility limit of transition metal oxides in mullite depends on an oxidation state and the radius of the substituted ion. Considering all these, it is thought that the reason for the c parameter increasing more is the presence of the Al^{3+} atom in the lower left corner of Fig.9. It can be said that this situation arises from the incorporation of Fe^{3+} atoms into the gap or their replacement with Fe^{3+} and Al^{3+}atoms.

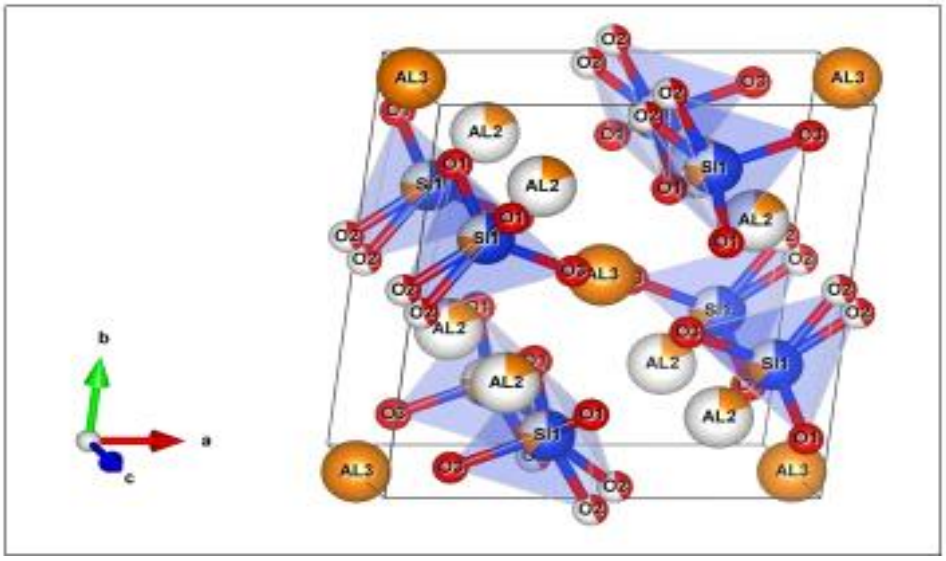

Fig 9. The unit cell of mullite in CC-31 clay.

In general, mullite crystals were seen in all microstructures (Fig.10 and Fig.11). Mullite grains had a strong tendency to grow anisotropically. The crystals formed have the appearance of whiskers or needles. The presence of iron and other impurities formed in the structure also had beneficial roles. They lower the temperature of the early formation of the liquid phase, which fills the pores between the grains and, as a result, improves the sintering process. At the same time, they increase the amount of liquid phase. The larger the crystals, the more controllable the liquid phase can be. Since the morphology and size of the formed mullite provide ease of work, the longer and larger the mullite structures, the more tolerable they are in the liquid phase. The needle-like morphology was typical for mullite with low iron content, while rod- or lath-like mullite grains occurred in mullite crystals with high iron content. The needle-like structures of the mullite in the SEM images are visible. The growth of mullite crystals increased as the iron ratios added to the body increased (Fig.13). At the same time, the growth of mullites is supported by the growth of crystal lattice parameters (Fig.7).

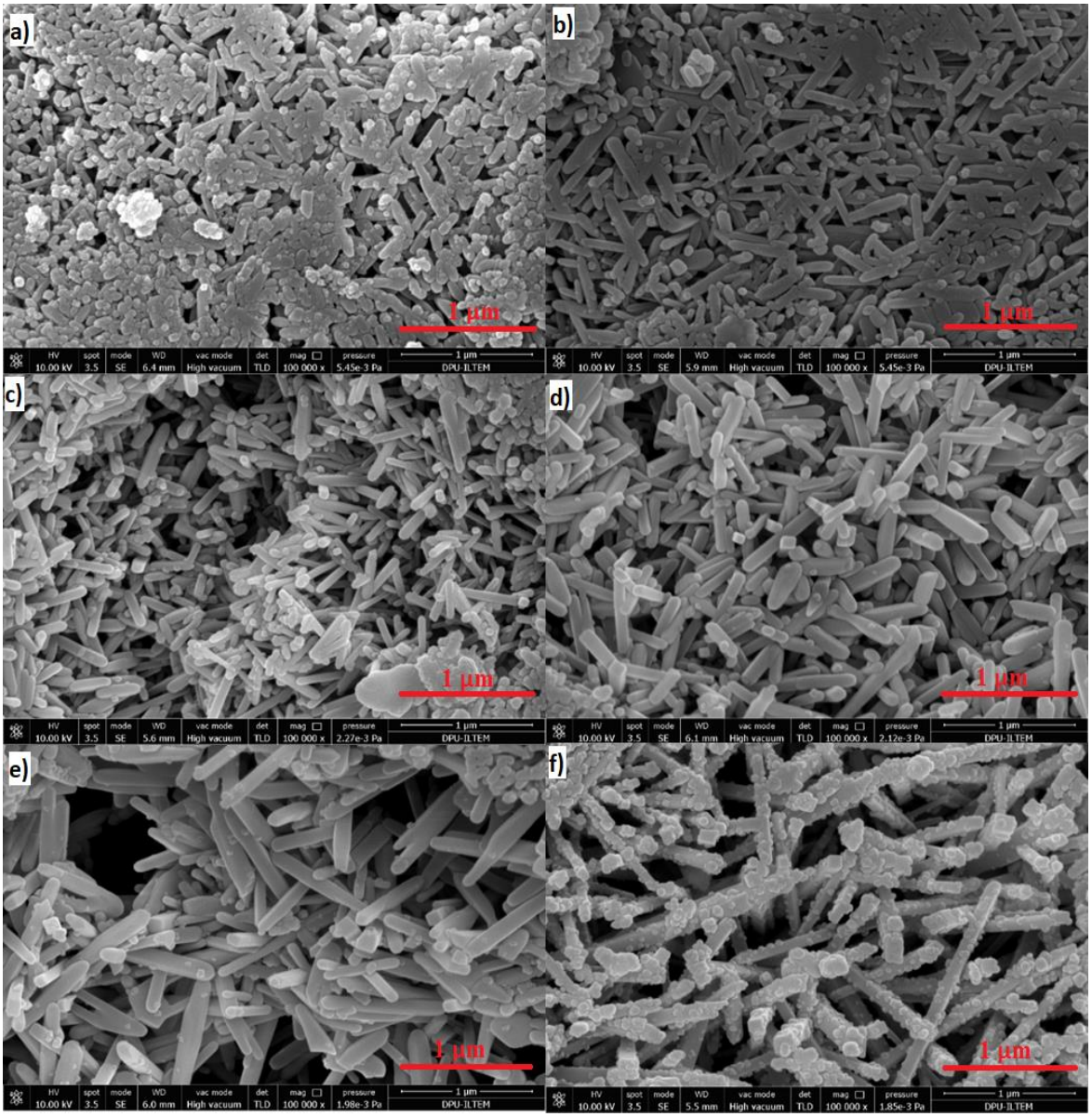

Fig 10. SEM images of (a) without addition CC-31 clay; (b) 2% Fe_2O_3; (c) 4% Fe_2O_3; (d) 6% Fe_2O_3; (e) 8% Fe_2O_3; (f) 10% Fe_2O_3 -added CC-31 clay.

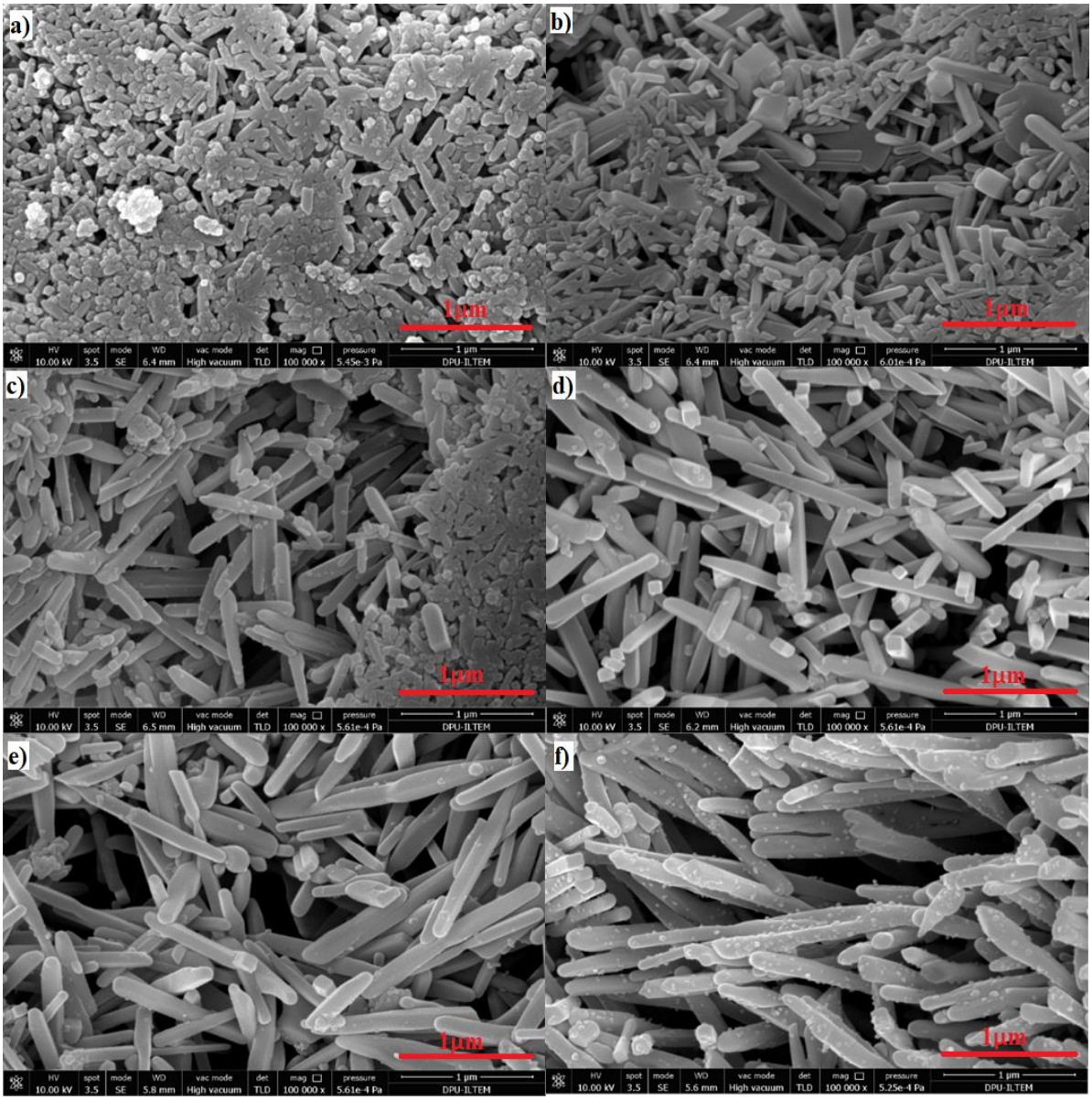

Fig 11. SEM images of (a) without addition CC-31 clay; (b) 2% $FeCl_3$; (c) 4% $FeCl_3$; (d) 6% $FeCl_3$; (e) 8% $FeCl_3$; (f) 10% $FeCl_3$ -added CC-31 clay.

In Fig.12 EDX analysis results of samples with 3% of Fe_2O_3 and 3% of $FeCl_3$ were given. The microstructures of the samples consisted of a high percentage of mullite crystals. According to EDX analysis, iron atoms were dissolved in mullite crystals, and this result is compatible with the mullite unit cell parameter.

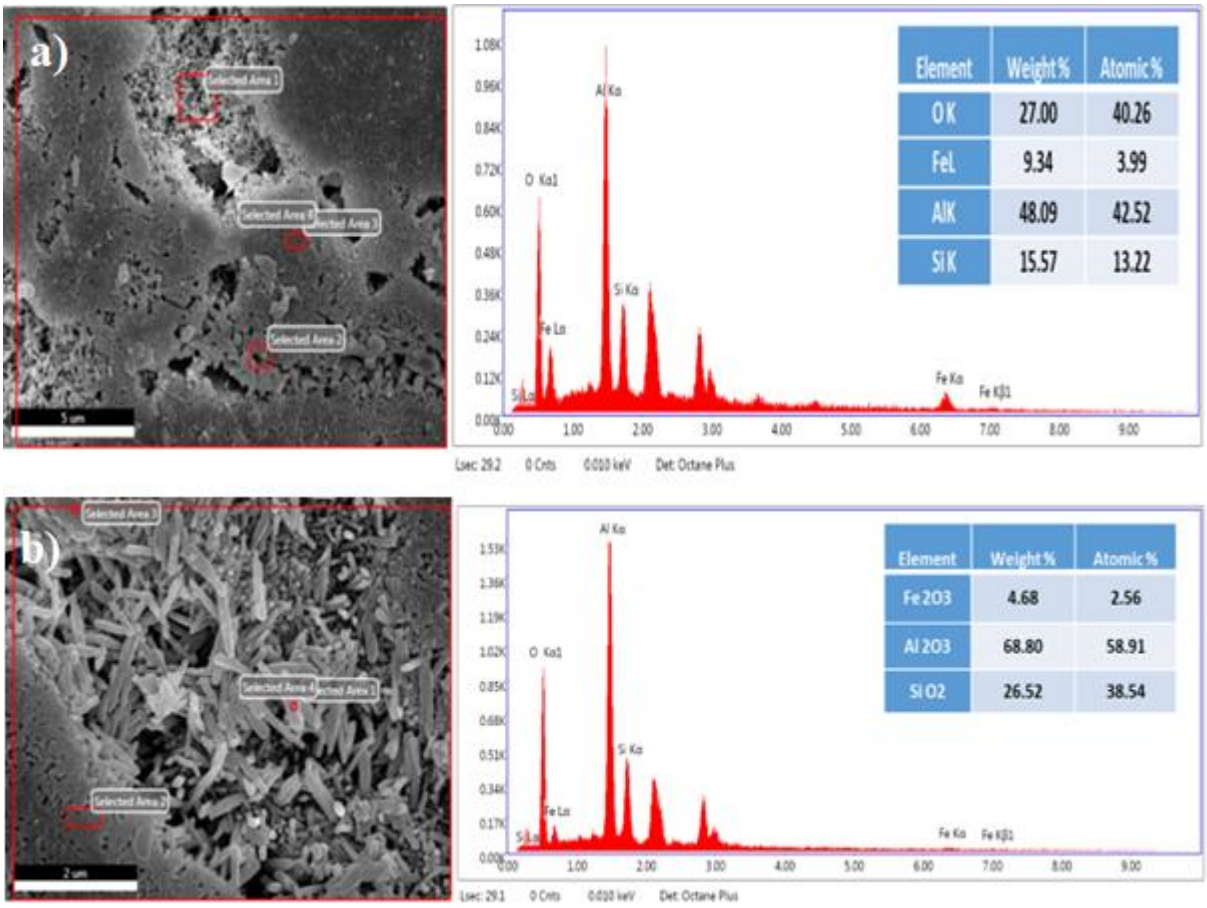

Fig 12. a) EDX analysis results of CC-31 clay with 3% Fe_2O_3 added by weight, b) EDX analysis results of CC-31 clay with 3% $FeCl_3$ added by weight.

In Fig. 13 the crystal growths depending on the iron source entering the structure of CC-31 clay were given. Mullite crystal size increases with the addition of both iron sources. Fe_2O_3 addition had a greater effect on mullite crystal size. Up to 4% addition, although the crystal size showed almost similar growth rates, the effect of Fe_2O_3 is more pronounced at 6% and 8% additions. Fe_2O_3 with an addition of 8%; caused the mullite crystal to grow 7.95% more.

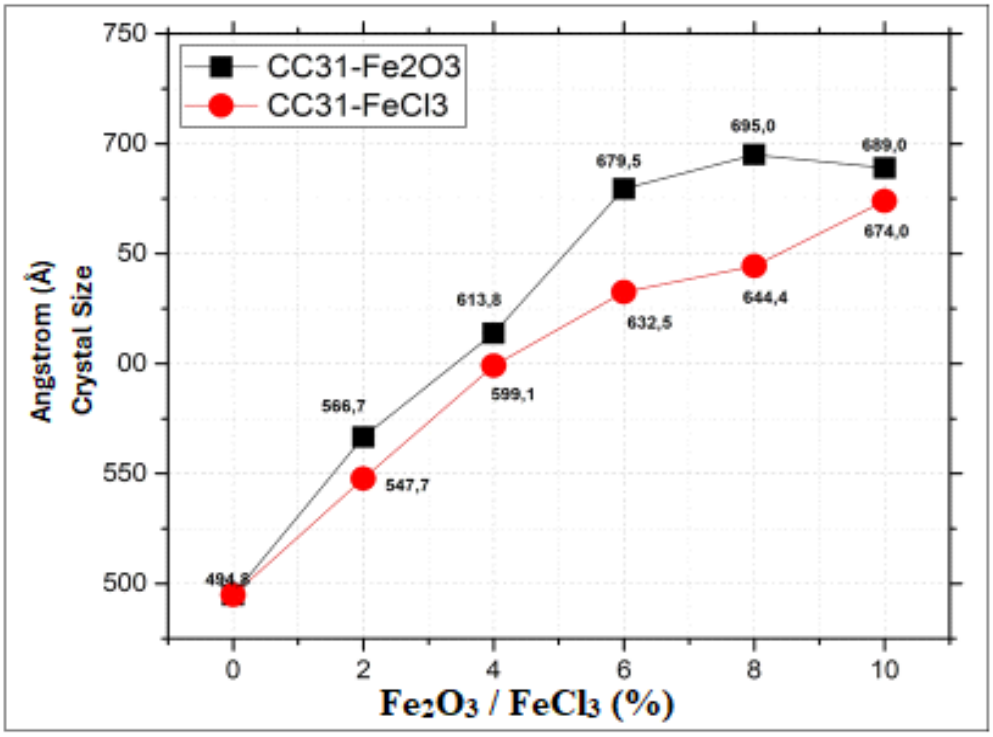

Fig 13. The crystal size of CC-31 clay doped with Fe_2O_3 and $FeCl_3$.

4. Conclusions

This study investigates the effects of iron sources on mullite formation, and color in clay and provides important information on the interaction between iron additives, and clay properties. The study comprehensively investigated how different concentrations of iron oxide (Fe_2O_3) and iron chloride ($FeCl_3$) affect mullite formation, color stability, and structural changes in CC-31 clay when sintered at 1200°C. This provided an understanding of how iron sources affect the mechanical and aesthetic properties of mullite containing ceramics, which are critical in various industrial applications. An important finding is that the high L* value, an indicator of the light color of the clay, is attributed to the high Al_2O_3 and low Fe_2O_3 content. Remarkably, the color of the clay remained almost unchanged with the addition of up to 2% Fe_2O_3 or $FeCl_3$. This suggests that small amounts of these iron sources do not significantly affect the color of the clay and maintain its desirable aesthetic qualities. The study also found a direct correlation between the addition of iron sources, the decrease in water absorption rates and the increase in mullite formation. As the iron content increased, the mullite crystals grew, indicating a favorable improvement in the structural properties of the material. With the addition of both Fe_2O_3 and $FeCl_3$ at 6%, the hematite phase began to appear, marking the threshold at which excess iron precipitates and is no longer integrated into the mullite structure. The study also found a direct correlation between the addition of iron sources, the decrease in water absorption rates and the increase in mullite formation. As the iron content increased, the mullite crystals grew, indicating a favorable improvement in the structural properties of the material. With the addition of both Fe_2O_3 and $FeCl_3$ at 6%, the hematite phase began to appear, marking the threshold at which excess iron precipitates and is no longer integrated into the mullite structure. The research concluded that the mullite phase formed after sintering CC-31 clay at 1200°C can incorporate up to 4-5% iron from both Fe_2O_3 and $FeCl_3$ sources into its crystal lattice. This incorporation capacity highlights the structural flexibility of mullite and its ability to maintain its formation while harboring significant amounts of iron. This results in an increased tolerance to red staining, a valuable property for ceramic applications where color consistency is critical. The findings not only contribute to a fundamental understanding of mullite formation but also pave the way for the development of advanced ceramic materials with special properties for specific industrial needs.

Acknowledgment

The authors acknowledge the financial support provided by Kütahya Dumlupınar University Scientific Research Projects Unit (KDPU-BAP), project No: 2022-61.

Author contribution

Z.G.S, and R.C.; Conceptualization, Methodology. Z.G.S, R.C, M.A.; Data curation, Writing- Original draft preparation, Visualization, Investigation. R.C, G.K., and F.S.; Writing- Reviewing and Editing.

References

[1] F. Gol *et al.*, "Evaluation of solid wastes in the manufacture of ceramic tableware glazes," *Ceram Int*, vol. 48, no. 11, pp. 15622–15628, Jun. 2022, doi: 10.1016/J.CERAMINT.2022.02.096.
[2] F. Gol *et al.*, "The use of boron based materials on efficiency of environmentally friendly porous ceramics," *Environ Res*, vol. 216, p. 114454, Jan. 2023, doi: 10.1016/J.ENVRES.2022.114454.
[3] A. De Bonis *et al.*, "Different shades of red: The complexity of mineralogical and physico-chemical factors influencing the colour of ceramics," *Ceram Int*, vol. 43, no. 11, pp. 8065–8074, Aug. 2017, doi: 10.1016/J.CERAMINT.2017.03.127.
[4] G. Yanik, F. Esenli, V. Uz, V. Esenli, B. Uz, and T. Külah, "Ceramic properties of kaolinized tuffaceous rocks in Kesan region, Thrace, NW Turkey," *Appl Clay Sci*, vol. 48, no. 3, pp. 499–505, Apr. 2010, doi: 10.1016/J.CLAY.2010.02.014.
[5] A. Akcıl and A. Tuncuk, "Kaolenlerin safsızlaştırılmasında kimyasal ve biyolojik yöntemlerin incelenmesi," *Kibited*, vol. 1, no. 2, pp. 59–69, 2006.
[6] Z. G. Sarıtas, "Farklı Tipteki Killerden Oluşturulan Mullit İçinde Demir Çözünürlüğünün Belirlenmesi," Kutahya, 2022.
[7] R. Ceylantekin and R. Başar, "Solid solution limit of Fe2O3 in mullite crystals, produced from kaolin by solid state reactions," *Ceram Int*, vol. 44, no. 7, pp. 7599–7604, May 2018, doi: 10.1016/J.CERAMINT.2018.01.178.
[8] H. Schneider, R. X. Fischer, and J. Schreuer, "Mullite: Crystal Structure and Related Properties," *Journal of the American Ceramic Society*, vol. 98, no. 10, pp. 2948–2967, Oct. 2015, doi: 10.1111/JACE.13817.
[9] J. Martín-Márquez, J. M. Rincón, and M. Romero, "Mullite development on firing in porcelain stoneware bodies," *J Eur Ceram Soc*, vol. 30, no. 7, pp. 1599–1607, May 2010, doi: 10.1016/J.JEURCERAMSOC.2010.01.002.
[10] C. Zhang, Z. Zhang, Y. Tan, and M. Zhong, "The effect of citric acid on the kaolin activation and mullite formation," *Ceram Int*, vol. 43, no. 1, pp. 1466–1471, Jan. 2017, doi: 10.1016/J.CERAMINT.2016.10.115.
[11] D. J. Duval, S. H. Risbud, and J. F. Shackelford, "Mullite," *Ceramic and Glass Materials: Structure, Properties and Processing*, pp. 27–39, 2008, doi: 10.1007/978-0-387-73362-3_2.
[12] A. Djemai, E. Balan, G. Morin, G. Hernandez, J. C. Labbe, and J. P. Muller, "Behavior of Paramagnetic Iron during the Thermal Transformations of Kaolinite," *Journal of the American Ceramic Society*, vol. 84, no. 5, pp. 1017–1024, May 2001, doi: 10.1111/J.1151-2916.2001.TB00784.X.
[13] H. Scheider, "Temperature-Dependent Iron Solubility in Mullite," *Journal of the American Ceramic Society*, vol. 70, no. 3, pp. C–43, Mar. 1987, doi: 10.1111/J.1151-2916.1987.TB04961.X.
[14] J. H. She and T. Ohji, "Fabrication and characterization of highly porous mullite ceramics," *Mater Chem Phys*, vol. 80, no. 3, pp. 610–614, Jun. 2003, doi: 10.1016/S0254-0584(03)00080-4.
[15] W. E. Brownell, "Subsolidus Relations Between Mullite and Iron Oxide," *Journal of the American Ceramic Society*, vol. 41, no. 6, pp. 226–230, Jun. 1958, doi: 10.1111/J.1151-2916.1958.TB13544.X.
[16] E. Elmas, "Mullit Oluşumunda Mekanik Aktivasyonun Etkisi," Sakarya Üniversitesi, Sakarya, 2009.
[17] W. E. Lee and Y. Iqbal, "Influence of mixing on mullite formation in porcelain," *J Eur Ceram Soc*, vol. 21, no. 14, pp. 2583–2586, Jan. 2001, doi: 10.1016/S0955-2219(01)00274-6.
[18] S. Ilić *et al.*, "Structural, microstructural and mechanical properties of sintered iron-doped mullite," *Materials Science and Engineering: B*, vol. 256, p. 114543, Jun. 2020, doi: 10.1016/J.MSEB.2020.114543.
[19] O. Castelein, R. Guinebretière, J. P. Bonnet, and P. Blanchart, "Shape, size and composition of mullite nanocrystals from a rapidly sintered kaolin," *J Eur Ceram Soc*, vol. 21, no. 13, pp. 2369–2376, Nov. 2001, doi: 10.1016/S0955-2219(01)00211-4.